AGU PUBLICATIONS

JGR

Journal of Geophysical Research: Atmospheres

RESEARCH ARTICLE

10.1002/2014JD021993

Key Points:

- A coupled weather-fire model simulated a Colorado wildfire during a windstorm
- Fine-scale air motions captured by the model shaped fire growth
- Satellite fire detection data and airborne fire mapping support the simulation

Supporting Information:

- Text S1
- Movie S1
- Movie S2

Correspondence to:
J. L. Coen,
janicec@ucar.edu

Citation:
Coen, J. L., and W. Schroeder (2015), The High Park fire: Coupled weather-wildland fire model simulation of a windstorm-driven wildfire in Colorado's Front Range, *J. Geophys. Res. Atmos.*, *120*, doi:10.1002/2014JD021993.

Received 7 MAY 2014
Accepted 8 DEC 2014
Accepted article online 11 DEC 2014

The High Park fire: Coupled weather-wildland fire model simulation of a windstorm-driven wildfire in Colorado's Front Range

Janice L. Coen[1] and Wilfrid Schroeder[2]

[1]National Center for Atmospheric Research, Boulder, Colorado, USA, [2]Department of Geographical Sciences, University of Maryland, College Park, Maryland, USA

Abstract Weather affects wildland fires at scales from multiseasonal precipitation patterns and anomalies, through synoptic and mesoscale weather patterns, to convective scale motions including fire-induced winds. This work analyzed the first day's growth of the 2012 High Park fire, which occurred in Colorado's Front Range during widespread drought and an unseasonal June windstorm, assessing to what extent the Coupled Atmosphere-Wildland Fire Environment coupled numerical weather prediction—wildland fire behavior model could reproduce the event, burn severity patterns, and how the drought impact on fuel moisture impacted the event. Simulated mountaintop wind speeds reaching 47 m s^{-1} and gravity wave overturning created strong, gusty surface winds. During the first 9 h, the simulated fire grew underneath the gravity wave's crest and downdraft, sheltered from the windstorm. The simulated fire then climbed a ridge, was exposed to the windstorm, and rapidly traveled east, covering 15 km in 12.3 h. Burning routed up or down drainages caused finger-like streaks in maximum fire intensity. Reference fire mapping information supported the simulated early growth toward the north, splitting around topographic features, while the simulation's underestimate of extent accrued to 2 km over 21.3 h. While the control simulation employed horizontal grid spacing of 123 m, a simulation refined to 370 m captured some wave motions and overall direction but further underestimated extent and lacked details such as turns in direction, splitting, or fingering at the leading edge. Compared to a simulation with moderately dry fuel conditions, a range of drought-like fuel moisture conditions produced fires that extended 0–39% farther.

1. Introduction

The June 2012 High Park wildfire, located near Fort Collins, Colorado, was ignited in historic drought conditions just before an unseasonal downslope windstorm. Burning 259 homes and 35,323 ha (87,284 acres) over its 3 week lifetime, it was the most destructive wildfire in state history at that time. The High Park fire exemplified the high-impact wildland fire event that can occur when multiyear climate anomalies such as a drought overlap a wind-producing weather event, causing both rapid fire spread and thorough fuel consumption leading to high-energy release rates. It repeated the June 2002 Hayman fire, Colorado's largest recorded fire, and foreshadowed the June 2013 Black Forest fire, its most destructive fire to date, when wildfires ignited in the Front Range during unseasonal June wind events raced predominantly eastward into wildland urban interface communities.

Windstorms occasionally occur along the eastern edge of the Rocky Mountains when synoptic conditions generate flow with a westerly (cross mountain) component throughout the troposphere (J. M. Brown, A decision tree for forecasting downslope windstorms in Colorado. Preprints 11th Conference on Weather Analysis and Forecasting. Amer. Meteor. Soc., Kansas City, 83–88, 1986) [*Mercer et al.*, 2008], accompanying wind speed and thermodynamic vertical profiles that establish internal gravity waves. These waves may steepen and break through processes which were explored by *Clark and Peltier* [1977], *Scinocca and Peltier* [1989], and others, creating extreme, gusty surface winds in the mountain's lee with gusts sometimes reaching 35–50 m s^{-1} [*Lilly*, 1978]. Climatologies show that these predominantly occur during December and January [*Julian and Julian*, 1969; *Whiteman and Whiteman*, 1974]; they infrequently record events reaching severe levels between April and September (an example is described in *Cotton et al*. [1995]), the period when fire danger levels peak. Thus, the superposition of this weather event upon a wildfire reflects a recently recognized and relatively unexplored regional hazard, although this shares similarities with Southern California wildfire events that occur when Santa Ana wind events [*Raphael*, 2003] overlap the local dry season.

Because these combined events have such impact, it is important that models capture how fire behavior may unfold in response to atmospheric conditions across multiple levels, including (i) the synoptic scale environment and mesoscale wind event that dominate interpretations of the High Park fire and (ii) atmospheric processes and scales of motion spanning down to submesoscale terrain-induced flow effects and convective scale feedback of the fire on the atmosphere and how multiyear drought affects the outcome.

In this work, the High Park fire evolution and environment are described, including synoptic scale weather down to convective scale terrain-induced flow effects. The CAWFE^{TM} coupled numerical weather prediction—wildland fire behavior modeling system was used to simulate the High Park fire in fuel conditions reflecting the widespread drought and the weather-fire dynamic interactions for 21 h during its first growth period. Complementary simulations show how the simulated outcome would differ using coarser grid spacing and under more moderately dry fuel moisture conditions rather than extreme drought. We discuss the implications for models that might be used to simulate similar wildland fire events.

2. The Wildfire and Its Environment

2.1. Drought Impact on Fuels

In 2012, climatologists increased estimates of the percentage of Colorado under drought conditions, based on the U.S. Drought Monitor (R. Heim, The U.S. Drought Monitor, http://droughtmonitor.unl.edu, 2014), from 50% to 100% as winter snow accumulation in mountainous regions was below average, spring temperatures were well above average, and precipitation was persistently below normal [*Ryan and Doesken*, 2012]. Measurements of the dead fuel moisture (DFM) of fine surface fuels, which respond rapidly to a dry atmospheric environment, varied across 84 Remote Automated Weather Stations (RAWSs) in Colorado from 2 to 4% at 23:00 UTC 9 June (5:00 P.M. MDT). Larger fuel components such as the 100 h and 1000 h DFM varied from 2 to 10% and 3 to 13%, respectively (Weather Information Management System, unpublished data, available at http://www.wfas.net, 2014). Near the burn area, the Red Feather RAWS reported 3%, 9%, and 12% as the 10, 100, and 1000 h DFM, respectively. At the same location, live fuel moisture, an indicator of canopy flammability and the slower response of living vegetation to seasonal moisture patterns, was around 85% in ponderosa pines, which is typically 92–101% at this time of year and approximately 90% in lodgepole pines, slightly below average (96%). The damage from mountain pine beetles was present in 28% of the burned area [*Hoffman et al.*, 2012], primarily in the southwestern quarter of the burn area, including scattered damage in the areas impacted during early fire growth, but especially in areas burned in later periods of the fire than this study examined.

2.2. Weather Environment

The High Park fire was ignited on 7 June by a lightning strike (40.589° latitude, −105.404° longitude) (S. Rudlosky, personal communication), 4 km to the east-southeast of East White Pine Mountain (40.605° latitude, −105.446° longitude, 3123 m above mean sea level (msl)) in the Rocky Mountains, approximately 30 km west of Fort Collins, in north central Colorado. It remained dormant until 9 June, when the fire was first reported at 11:54 UTC 9 June (5:54 A.M. mountain daylight time (MDT)) (Inciweb, http://inciweb.nwcg.gov/incident/2904/, 2014) as winds increased during the onset of a windstorm. The 300 mb analyses (Figure 1a) from 15:00 UTC 9 June indicated that the polar jet had moved farther south than usual and a trough over the Great Basin associated with a stationary front produced strong southwesterlies throughout the troposphere over Colorado. The 12:00 UTC 9 June atmospheric sounding at Grand Junction, Colorado, upwind of the event, indicated strong cross-mountain winds, a stable layer, and vertical wind shear (Figure 1b). This large-scale weather environment resembled optimal conditions associated with wintertime Front Range windstorms [*Doyle et al.*, 2000] and previously noted unseasonal summer windstorms [e.g., *Cotton et al.*, 1995]. Eighteen hours later, near the end of the fire's initial growth period, upper level winds had increased but had shifted to south-southwesterly with less of a cross-mountain component (Figure 1c).

Throughout the fire, 1–4 day periods of strong, gusty winds with diurnal variability occurred during which most of the fire growth was recorded (K. Gollnick-Waid et al., Fire behavior and fire weather assessment, high park fire, unpublished report, 14 pp., 2012). Surface weather data that would show winds over the fire area are limited to two surface weather stations—Redstone (40.571° latitude, −105.227° longitude) and DW4366 Red Feather (40.771° latitude, −105.476° longitude)—that lay in the forested hills approximately 15.1 km downwind

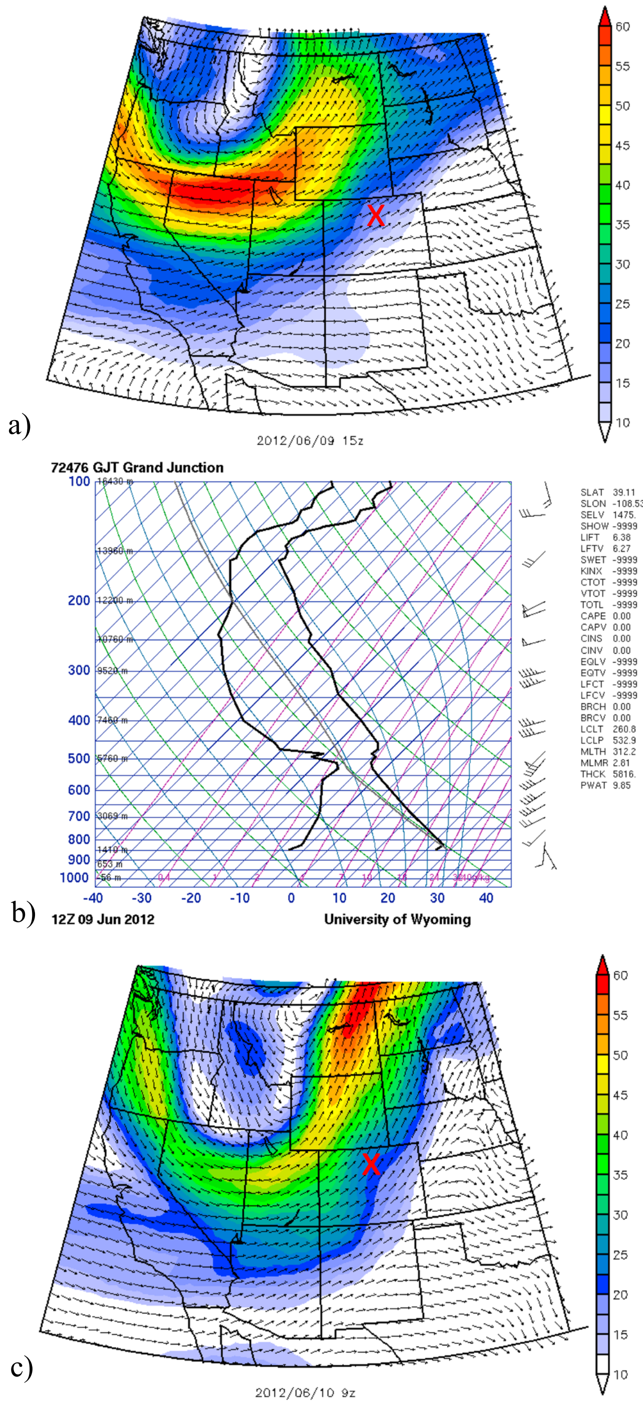

Figure 1. The NCEP North American Regional Reanalysis vector wind at 300 mb at (a) 15:00 UTC 9 June 2012, and (c) 15:00 UTC 10 June 2012. The arrows indicate wind direction with the wind speed (in m s^{-1}) given by the color bar at the right (from the National Oceanic and Atmospheric Administration Physical Sciences Division). The ignition location is indicated by "X." (b) Atmospheric profile at Grand Junction, Colorado, at 12:00 UTC 9 June 2012 (courtesy of the University of Wyoming).

and 21.1 km north-northwest of the ignition. A 14 h surge in winds began approximately at the time of first report in both these stations and downwind of the fire along the Front Range in Fort Collins (40.641° latitude, −105.105° longitude), peaking between 18:00 and 20:00 UTC and subsiding until between 02:00 and 04:00 UTC 10 June (Figure 2). In these stations, sustained winds reached 6–9 m s^{-1}, with intermittent gusts reaching 11–14 m s^{-1}. A second 16–18 h period of stronger (12–16 m s^{-1}) and gustier (19 m s^{-1}) winds followed at Red Feather Lakes and Fort Collins, peaking at about 10:00 UTC on 10 June and lasting until 20:00 UTC 10 June.

2.3. High Park Fire Event

The evolution of fire growth during the study period comes from satellite active fire detection data, airborne imaging, and intelligence collected by the incident team (Figure 3). The Visible Infrared Imaging Radiometer Suite (VIIRS) on the Suomi National Polar-orbiting Partnership delineated the wildfire's flaming front with 375 m active fire detection data collected twice daily [*Schroeder et al.*, 2014], providing routine observations at approximately 2:30 P.M. and 2:30 A.M. MDT in this study area. VIIRS first detected the High Park fire on its pass at 20:19 UTC 9 June (2:19 P.M. MDT), at the peak in the first windy period (Figure 2), 8.25 h after the first report, showing a 4.0 km long wedge spreading to the northeast.

At 04:12 UTC 10 June (10:12 P.M. MDT 9 June), a U.S. Department of Agriculture National Infrared Operations (NIROPS) map produced by an airborne infrared mapping instrument showed that during the next 8 h, as the winds and gusts were decreasing from their first peak (Figure 2), the fire had spread northward toward Poudre Canyon, turned toward the east, and traveled 8 km generally downslope across two ridges. At approximately 05:00 UTC 10 June (11:00 P.M. MDT 9 June), the incident management team noted that a structure in Poudre Park had been ignited. The second VIIRS detection at 08:37 UTC 10 June (2:37 A.M. MDT), which occurred just as the winds were peaking in the second, stronger surge of winds (Figure 2), showed that the fire had arced

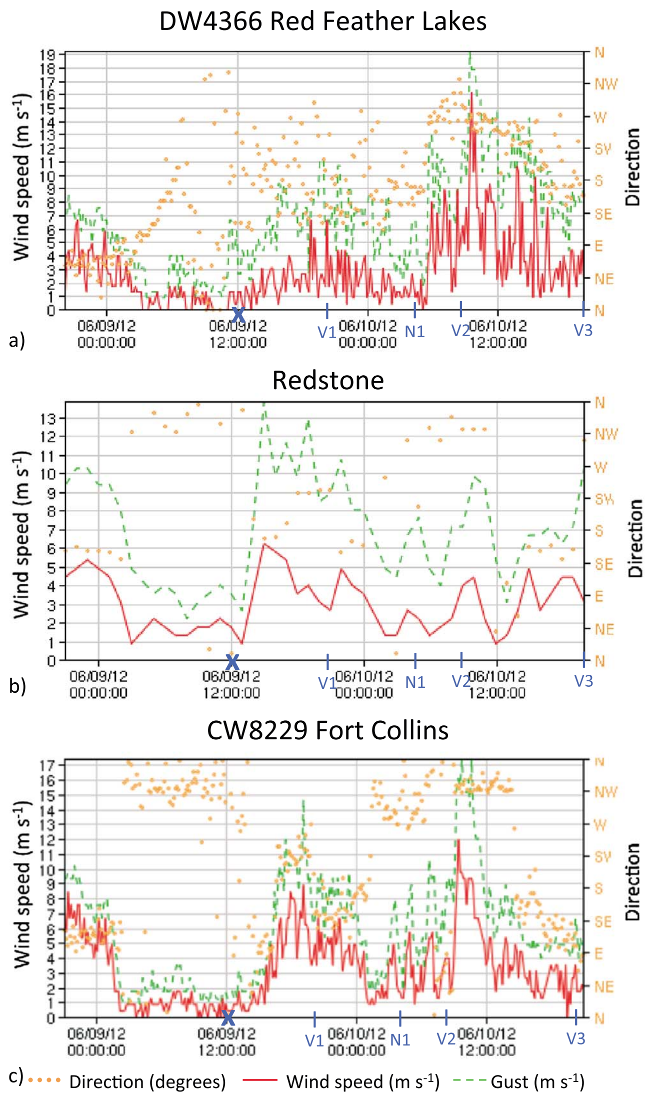

Figure 2. The wind speed, gust, and direction as functions of time (UTC) at the (a) DW4366 Red Feather Lakes APRXWXNET/Citizen Weather Observing Program surface station (10 m agl), (b) Redstone RAWS (6.66 m agl), and (c) CW8229 Fort Collins APRXWXNET/Citizen Weather Observing Program surface station (10 m agl) from Mesowest. *X* indicates the time of first report. V1, V2, V3, and N1 indicate when the first three VIIRS and the first NIROPS observations (shown in Figure 3) were collected.

10 km farther eastward. Incident reports of burning structures corroborated that the fire had reached the foothill/plain interface by 10:00–11:00 UTC 10 June (4:00–5:00 A.M. MDT) (K. Close, personal communication) and that a wider area than indicated by the NIROPS map had burned (K. Close, personal communication). The second surge of winds driving growth had ended near this time; the burned area in the third VIIRS image at 20:00 UTC 10 June (2:00 P.M. MDT) was only slightly larger than in its prior pass, although the next NIROPS map at 06:20 UTC 11 June (12:20 A.M. MDT 11 June) showed another substantial increase in the fire-affected area to the south. The fire burned for 3 weeks, progressing during multiday windy periods interrupted by lulls, primarily along the south flanks and to the west.

3. Materials and Methods

3.1. The CAWFE Coupled Numerical Weather Prediction–Wildland Fire Behavior Model

CAWFE couples a numerical weather prediction model designed for simulations at horizontal grid spacing at tens through thousands of meters in complex terrain with a fire behavior module. The numerical weather prediction model within CAWFE [*Clark and Hall*, 1991; *Clark et al*., 1996, 1997] is nonhydrostatic and based on the Navier-Stokes equations of motion, a thermodynamic equation, a conservation of mass equation using the anelastic approximation, and prognostic equations for water vapor and precipitation fields. It is initialized with gridded model analyses (for past events) or forecasts (in a predictive mode) from larger-scale global weather models. Vertically stretched terrain-following coordinates allow detailed simulation of airflow at horizontal resolutions of hundreds of kilometers while telescoping in to focus at tens to hundreds of meters in complex terrain. Very steep slopes or sharp transitions in terrain may increase model error and create numerical instability, respectively. In practice, filters applied to both the model terrain and its gradients and the pressure solver described in *Clark* [2003] keep the residual numerical divergence at minimal levels. The outer of several interactive, nested modeling domains are initialized, and boundary conditions are updated with gridded atmospheric states from model forecasts or analyses. It has been implemented with both shared memory [*Clark et al*., 1996] and distributed memory [*Clark et al*., 2003] parallelization. It has previously been applied over 35 years to topics including terrain-induced turbulence, cloud entrainment, orographic, winter, convective precipitation, desert meteorology, convective initiation, and most relevant to this work, mountain gravity waves and downslope windstorms [*Clark and Peltier*, 1977; *Peltier and Clark*, 1979; *Clark et al*., 2000;

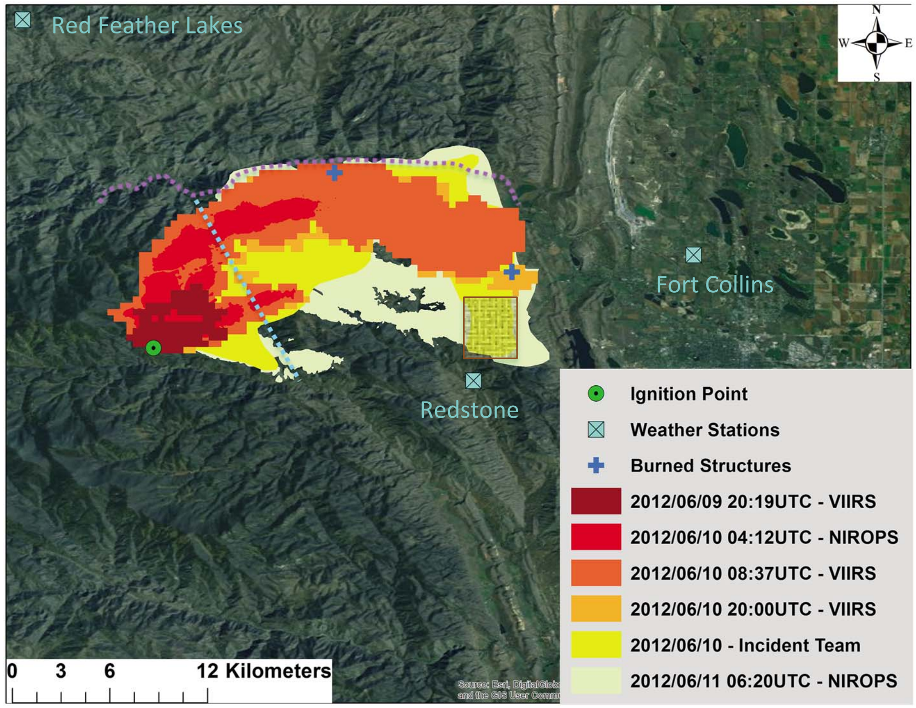

Figure 3. Maps and point indicators of fire extent during the High Park fire's first growth period until 06:20 UTC 11 June (12:20 A.M. MDT 11 June) from different sources, identified in the figure legend, in chronological order: (1) the 7 June ignition point, (2) the 20:19 UTC 9 June (2:19 P.M. MDT) VIIRS active fire detection polygon (V1 in Figure 2), (3) the USDA Forest Service airborne NIROPs at 04:12 UTC 10 June (10:12 P.M. MDT) (N1 in Figure 2), (4) a structure reported by the incident team to have been ignited at Poudre Park ("+" at the top) at approximately 05:00 UTC 10 June (11:00 P.M. MDT 9 June), (5) the 08:37 UTC 10 June (2:37 A.M. MDT 10 June) VIIRS polygon (V2 in Figure 2), (6) a structure that was reported by the incident team to have been ignited at Cloudy Pass (+ at the right) at 10:00–11:00 UTC 10 June (4:00–5:00 A.M. MDT), (7) the extent estimated by the incident team at approximately 11:00–12:00 UTC 10 June (5:00–6:00 A.M. MDT), (8) the 20:00 UTC 10 June (2:00 P.M. MDT) VIIRS polygon (V3 in Figure 2), and (9) the NIROPs map at 06:20 UTC 11 June (12:20 A.M. MDT). Three weather stations mentioned in the text are also shown—(top left) DW4366 Red Feather, (center) Redstone, and (right) CW8229 Fort Collins. The cross hatch on (7) indicates growth south along the foothill-plain interface that was later determined to not have occurred until later on 10 June. The dashed lines indicates Buckhorn Road (blue) and Poudre Canyon (magenta).

Parker and Lane, 2013] to explain their three-dimensional aspects [*Clark et al*., 1994], along-ridge flow [*Clark et al*., 1994] and variability [*Clark and Farley*, 1984], temporal variability such as pulsing behavior [*Scinocca and Peltier*, 1989], and requirements for operational simulation [*Sharman et al*., 2004].

The fire module treats the propagation of a wildland fire in response to the terrain's slope, the evolving weather, and fuel type and state as impacted by weather. CAWFE does not explicitly simulate flames or combustion but parameterizes these subgrid-scale processes with semiempirical and empirical relationships. These are described in *Coen* [2005], and detailed equations are given in *Coen* [2013]. In summary, near-surface atmospheric winds are used to calculate the direction and spread rate of the fire, which releases sensible heat, latent heat, and smoke into the lower atmosphere at rates that vary in space and time according to the fuel consumption rate. The fire's heat fluxes alter the atmospheric state, including winds directing the fire. Fire module algorithms treat physical processes on two-dimensional fuel cells on the surface that are further refined from atmospheric grid cells. These processes include the surface fire flaming front's rate of spread, postfrontal heat release, the ignition and propagation of a crown fire through the tree canopy and rate of canopy consumption, and upscaling of heat fluxes and distribution within the lowest layers of the atmospheric model. An additional algorithm defines the subgrid-scale interface between burning and unignited fuel as it passes through fuel cells.

Energy from the surface fire is first used to heat and dry any canopy above a surface fire. A crown fire was ignited in the simulation if, after heat is used to ignite and dry any canopy fuel in its grid (thus introducing a dependence on the foliar moisture content), the critical surface fire intensity remaining exceeded a prescribed threshold of 170 kW m^{-2}, an approach similar to that proposed by *Van Wagner* [1977], who specified the minimum surface fire intensity needed to ignite a crown fire in terms of the height of the canopy fuels and the foliar moisture content. When crown fires occur, occasions during which they travel at separate rates of spread from the surface fire are rare and transient (D. Sandberg, personal communication). Thus, if the criteria for igniting a crown fire are locally met, the crown fire and the surface fire are assumed to spread together at a rate that is a multiple of the predicted surface fire rate of spread in forest litter fuels, based on *Rothermel*'s [1991] analysis deriving rates of spread for long-duration crown fire runs in coniferous forests of the western U.S. *Scott* [2006] details the dependencies and sensitivity of *Rothermel*'s [1991] and other crown fire rate of spread treatments, notably *Cruz et al*. [2005], which arose from much shorter duration experimental crown fires in Canadian forests [*Scott*, 2006]. Although the relationship given in *Cruz et al*. [2005] additionally depends weakly on the crown bulk density, both approaches depend on fuel moisture through the estimated fine dead fuel content. A limitation is that these parameterizations clearly oversimplify very complex dynamics within crown fires, which are known to vary in time and space [*Taylor et al*., 2004] and progress in bursts [*Coen et al*., 2004] and are thus unlikely to be well represented by simple linear relationships.

Once ignited, we assume that the canopy fuel load (specified initially as 1.121 kg m^{-2}) decreases linearly over the canopy burn-out time, which is 1, 2, or 3 min for canopies associated with surface fuel models 8, 9, and 10, respectively. Based on the energy content of dry fuel, this rate of energy release is converted to an energy release rate per unit area or crown fire sensible heat flux. Then, based on the canopy's mass loss, live fuel moisture, and the water content of cellulosic fuels, a latent heat flux is calculated as described in *Coen* [2013].

One or several fires can be ignited within the model as points, corresponding to lightning strike locations or time and location of first reports, or "in progress" using a gridded map of fire extent [*Coen and Schroeder*, 2013], obtained from satellite or airborne data or incident team intelligence. It has been applied to over a dozen landscape-scale fires in varying terrain, fuel, and weather conditions [e.g., *Coen and Riggan*, 2014].

3.2. Application to the 2012 High Park Fire

National Centers for Environmental Prediction (NCEP) Final Operational Global Analysis-gridded atmospheric data were used to initialize the atmospheric state and provide boundary conditions for a two-domain (30 km and 10 km horizontal grid spacing) Weather Research and Forecasting (WRF) simulation begun at 03:00 UTC 9 June (9:00 P.M. MDT on 8 June). The WRF simulation dynamically downscaled the analyses to provide initial conditions and lateral boundary gradients of winds, temperature, and other atmospheric state variables for CAWFE at 1 h intervals. In the primary experiment (5D_06_75), CAWFE employed five nested domains telescoping from the western U.S. to the Colorado Front Range with horizontal grid resolutions of 10 km, 3.3 km, 1.1 km, 370 m, and 123 m. The vertical grid was stretched; the maximum vertical grid spacing in the innermost domain was 200 m above 2.5 km above ground level (agl). The first two vertical grid levels above ground were 23.3 and 57.8 m, with the first half-grid level (where horizontal wind components are located) at 11.7 m agl. The outermost domain's top was 20.8 km agl, domain 4's top was 12.2 km agl, and domain 5's top was 5.8 km agl. Time steps varied from 30 s for the outer domain to under 1 s for the fifth domain.

The CAWFE simulation period extended from 06:00 UTC 9 June (12:00 A.M. MDT on 9 June) to 09:15 UTC 10 June (3:15 A.M. MDT), simulating the weather during the night preceding the first report, the fire growth from the first report at 11:54 UTC 9 June (5:54 A.M. MDT), and interacting weather and fire for the next 21:21 h until this growth period ended. Simulated and observed fire extents were compared at times when mapped data or incident team estimates were available.

From west to east, the terrain elevation in domains 4 and 5 (Figure 4a) decreased from the Continental Divide (4101 msl.) to the high plains (1531 m msl). The High Park fire traversed a range of ecosystems, from varied conifer forests with abundant surface debris at higher elevations near its origin to mixed shrubs and grassy meadows at lower elevations, presenting a complex fuel mosaic. The spatial distribution of surface fuel models, categorized using *Albini*'s [1976] classification system as restated by *Anderson* [1982] (Figure 4b), was obtained from Landscape Fire and Resource Management Planning Tools Project (LANDFIRE) (unpublished data, 2014) available from the U.S. Department of Agriculture, Forest Service and U.S. Department of Interior (http://www.landfire.gov) and resampled to model fuel cells (5 × 5 lay within the footprint of each atmospheric grid cell) using nearest-neighbor resampling. *Anderson* [1982] offers sets of values of physical

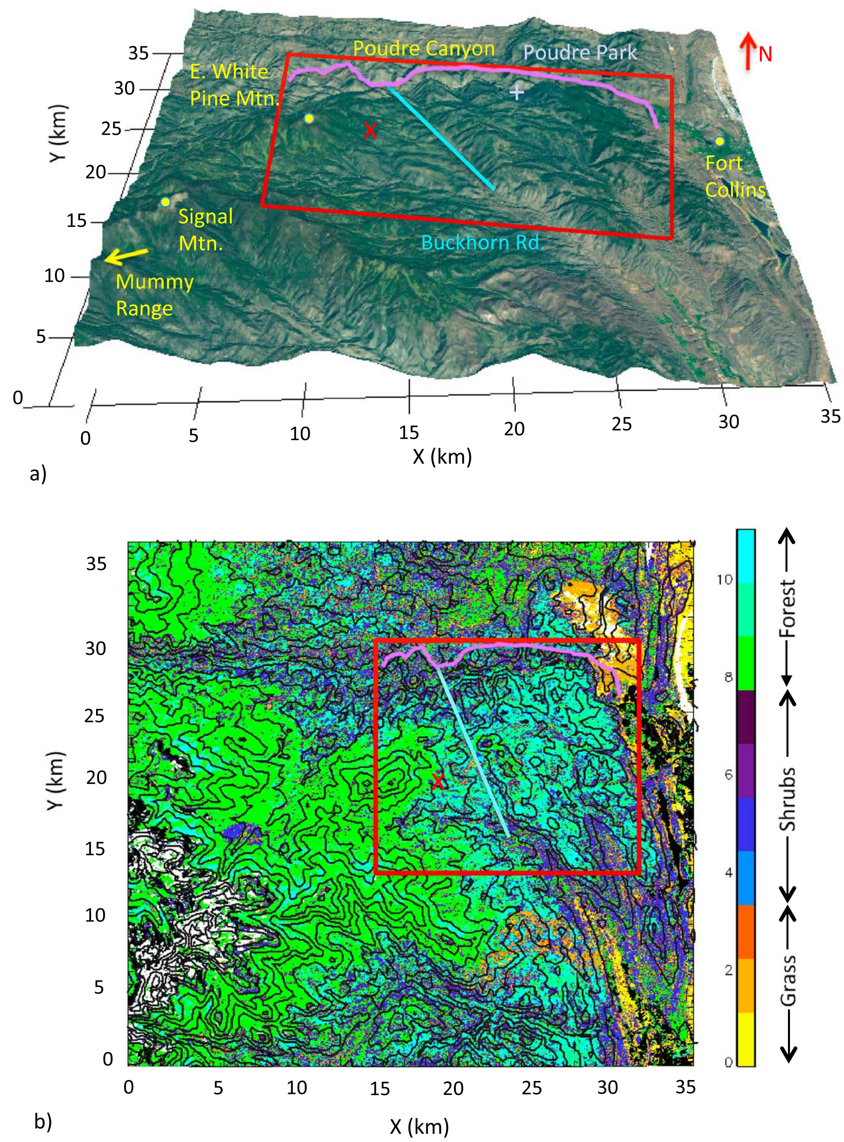

Figure 4. (a) Three-dimensional map showing terrain and (b) spatial variability of fuel models, with terrain contours every 150 m, in the fourth and fifth (indicated by red outline) domains. In each figure, the ignition location is shown with a red *X*. The superimposed lines indicate Buckhorn Road (blue) and Poudre Canyon (magenta).

properties including fuel load, fuel bed depth, surface area to volume ratio, and moisture of extinction for each of these stylized fuel models; however, it must be noted that actual values may vary from these and, in addition, even within a unit classified as a single fuel model; loads and other properties may vary. It is possible that these uncertainties in actual fuel properties may affect simulated fire outcomes. A prior case study [*Coen and Riggan*, 2014] that was also characterized by strong winds showed that using fuel loads derived from remote sensing data had little impact on the fire's shape, character, and growth. Tests on other parameters had similarly small effects; however, *Coen and Riggan* [2014] noted that in the absence of strong ambient or fire-induced winds, a modeled fire's character could be relatively more sensitive to variations in fuel properties.

Additional experiments were used to test model sensitivities. For example, as *Doyle et al.* [2000] noted, spatial resolution impacts results; thus, Experiment 4D-06_075 implements only four nested domains to 370 m horizontal grid spacing, not five, to show the effect that the additional horizontal grid refinement was produced. As noted in section 2.1, the fine fuel DFM varied widely across Colorado. A weakness in the input data is that this spatial variability is not captured due to the sparseness of the fuel moisture measurements

Table 1. Experiments Referred to in Text

Experiment	Finest Horizontal Grid Spacing (m)	Fine Dead Fuel Moisture (%)	Live Fuel Moisture (%)
5D_06_075	123.	6 ± 2.	75.
4D_06_075	370.	6 ± 2.	75.
4D_06_090	370.	6 ± 2.	90.
4D_04_090	370.	4 ± 2.	90.
4D_04_075	370.	4 ± 2.	75.
4D_08_110	370.	8 ± 2.	110.

and weather station data from which it may be diagnosed. This uncertainty effect on fire behavior is examined through experiments that vary the live and dead fuel moisture (see Table 1); these experiments are varied around the four-domain configuration due to the approximately 9 times larger computational cost of the five domain configuration. In the primary experiment (5D_06_075) shown in later figures and its four-domain version (4D_06_075), the dead fine fuel moisture content was specified as 6%, with a sinusoidal diurnal pattern peaking (minimizing) at 8% (4%) at 3:30 A.M. (3:30 P.M), respectively, and the canopy's live fuel moisture was set as 75%, 10–15% lower than biweekly observations recorded and the lowest of this work's live fuel moistures. *Jolly et al*. [2012] described how the foliar moisture content is reduced in lodgepole pine during the early stages of beetle attack, and although areas affected by bark beetles were limited to the areas of early fire growth and otherwise southwest of the region of this study, this experiment might simplistically suggest how fire behavior would vary with the resulting lower foliar fuel moistures. Other experiments employ a lower dead fine fuel moisture content (4%), a higher live fuel moisture content in accordance with observations (90%), and an experiment in which the dead fine and live fuel moistures corresponded to the moderately dry conditions specified in *Schoennagel et al*. [2012], i.e., not during a prolonged drought. An experiment configured like 4D_06_075 but without a fire was run, and the mathematical differences between its wind components and scalar fields and those of 4D_06_075 were calculated to quantify the fire's effect on the atmospheric state, as done in *Coen* [2005]; however, this difference analysis was not effective in this flow regime and is not shown. Simulations of breaking gravity waves are thought to be highly nonlinear [*Peltier and Clark*, 1979], and thus, as anticipated, the difference fields show a disproportionate disruption from the fire throughout the domain from which actual fire effects cannot be determined.

4. Results

The airflow regime in this event was characterized by the formation and breaking of mountain gravity waves with three-dimensional, time-evolving features. As stated earlier, this windstorm resembled previous Front Range windstorms, the structure of which has been studied with NWP models including the one used in this work. This work builds on the prior studies such as *Clark et al*. [2000], who found that capturing the full range of motions from synoptic down to convective scale (100 to 200 m) was required in order to reproduce the variability of the windstorm dynamics and the local flow, which, in this work, impacts fire growth.

The windstorm during the High Park fire occurred in periods of 1–4 days (K. Gollnick-Waid et al., unpublished report, 2012). During the first growth period, the air impacting the newly reported fire was stably stratified throughout the troposphere with winds from the west-southwest largely orthogonal to the north-south oriented mountains with a weaker along-ridge component. As the stratified flow was lifted over complex terrain, gravity waves formed. The vertical structure was characterized by a high-speed layer near the surface with wind speed maxima reaching 47 m s^{-1} over East White Pine Mountain (3123 m) approximately upwind of the fire's ignition (Figure 5a). Wave breaking occurred at times when air with lower potential temperature was lifted into faster moving air aloft, tilting denser air over less dense air with higher potential temperature below (Figure 5b). This overturning and wave breaking resulted in pulses of energy transported downward to the surface (Figure 5c), creating a 1–2 km deep layer of turbulent, gusty winds. The upstream conditions varied with time, notably changing the wind's orientation to the north-south mountain range, sometimes heightening, shifting, or eliminating the wave, the downdraft, and the jump region (similar to *Lilly and Zipser* [1972]). During the first few hours after first report, the simulation showed a gravity wave produced in air flowing over East White Pine Mountain, with the crest of the wave and occasionally its downdraft directly over the fire (as in Figure 5a), overlying a narrow, shallow (under 1 km wide and deep), shifting

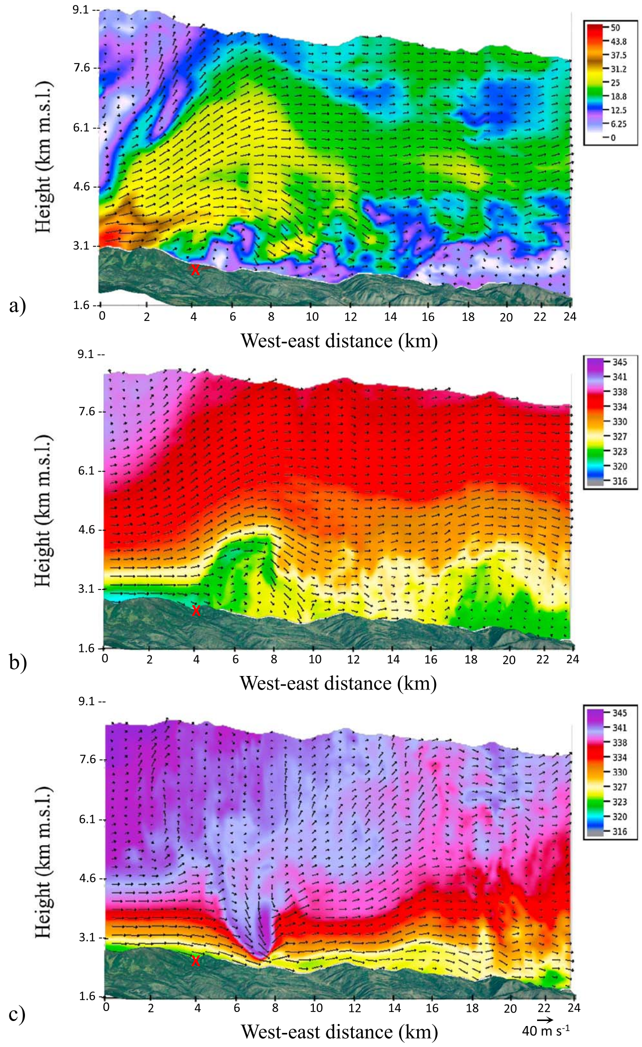

Figure 5. Vectors indicate simulated wind in the plane through domain 5. (a) West-east vertical cross section through windstorm maximum atop East White Pine Mountain. Wind speed in the plane (in m s^{-1}) at 11:48 A.M. MDT 9 June, contoured according to the color bar. (b) West-east vertical cross section through ignition. Potential temperature (in K) at 11:20 A.M. MDT 9 June contoured according to color bar. (c) Same as in Figure 5b at 6:17 P.M. MDT 9 June. Ignition location is indicated with red *X*.

region in which the west-east wind component remained less than a few m s^{-1}. Thus, the fire itself was sheltered from the strong sustained windstorm winds and instead experienced intermittent gusts to the north/northeast coming from upwind peaks to the southwest including Signal Mountain (3400 m) and peaks in the Mummy Range (approximately 4100 m). These weak gusts caused the fire to spread north/northeast as was observed during the early periods. These two distinct flow regions—strong, near-surface windstorm winds and the sheltered region east of East White Pine Mountain—can be seen in Figure 6a.

The simulated fire extent at 2:19 P.M. MDT (Figure 6a) resembled the first VIIRS data at this time (Figure 3), shaped like a 4.0 km long wedge (versus 4.0 km long in the observation). The simulated fire climbed a short ridge west of Buckhorn Road into a wildland urban interface area, split at the same location as seen in the 04:12 UTC 10 June (10:12 P.M. MDT 9 June) NIROPS map (Figure 3) into two heading regions (Figure 6b). At this point, the southern heading region's extent was under simulated by 1.5 km. The difference may be attributed to fuel, terrain, or winds or some combination of these factors. The fire line was descending through fuels transitioning between forest to sparse shrub to a lower-lying wildland urban interface area dominated by grass and crosscut with forested hillocks, while the thumb-like southern heading region was limited from growing across a local boundary between windstorm winds into weak gusts. The simulation underestimated the leading edge of the northern heading region by 2.2 km at this time compared to the NIROPS map but showed (as 5 km) the wider (N-S) burning area in the center recorded by the incident team (7.5 km) than the narrow bands (2 and 3 km wide) separated by scattered burning that NIROPS reported. The fire's growth north to Poudre Canyon and east to the interface of the foothills with the plains in the next 4.5 h as mapped by VIIRs (Figure 3) was also seen in the simulation, although it continued to lag observations by 2–3 km.

The structure of modeled winds and waves varied spatially from south to north, reflecting the variation in upwind topography and cores of cross-mountain wind created by the along-ridge component of motion (Figure 7). As a result, during the first few hours after first report, there was more steepening and consequent sheltering from the southern end of domain 5 to several kilometers north of the fire; north of this, high-speed winds frequently flowed close to the ground, producing stronger near-surface winds (Figure 6a). As the simulated fire grew north and its east flank climbed parallel but lower elevation north-south oriented ridges, it was exposed to strong near-surface westerlies causing its eastern flank to grow, presenting a north-south

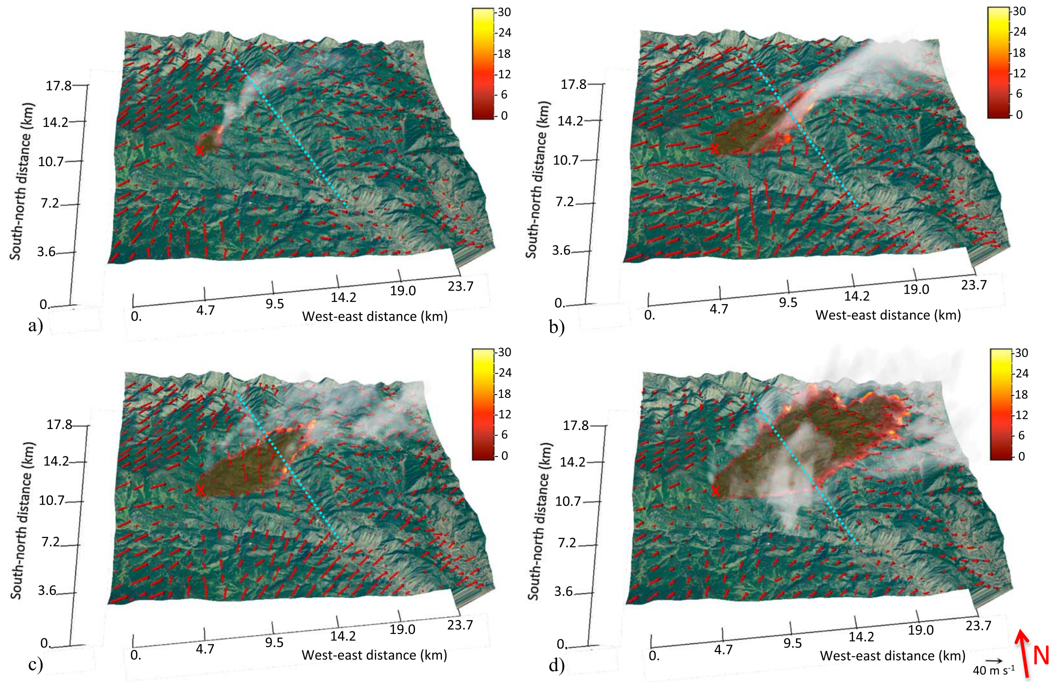

Figure 6. Three-dimensional map of fire heat flux in domain 5 (colored according to color bar at right, in kW m^{-2}), with wind vectors near the surface, at (a) 20:19 UTC 9 June (2:19 P.M. MDT), the time of the first VIIRS data (Figure 3); (b) at 02:33 UTC 10 June (8:33 P.M. MDT 9 June), showing two heading regions as in the NIROPS map 1.6 h later; (c) 04:12 UTC 10 June (10:12 P.M. MDT 9 June), the time of the NIROPS map; and (d) at 08:37 UTC 10 June (2:37 A.M. MDT), the time of the second VIIRS data. The misty white field indicates modeled smoke, where darker and denser locations represent higher concentrations. The dashed blue line indicates Buckhorn Road, and the *X* indicates the ignition location.

oriented flank that spread rapidly east. The wind storm weakened and the strength and locations of near-surface wind speed maximums and minimums changed as the synoptic scale wind veered to a less orthogonal orientation with respect to the Rocky Mountains between Figures 1a and 1c.

Differences between the simulation and mapped fire primarily lie in downwind extent, which lagged in the simulations by a few kilometers during the period of rapid growth, and in the center, over Buckhorn Road, where modeled results overestimated the fire extent detected by NIROPS, but agreed with wider estimates of burned area noted by the incident team. In addition to weaknesses in the simulated winds or fire behavior, these could be due to fire protection of wildland urban interface areas on Buckhorn Road and underestimates of fire extent by infrared mapping tools which may occur in fast-moving fires in light, patchy grass, or shrubs on clay soils.

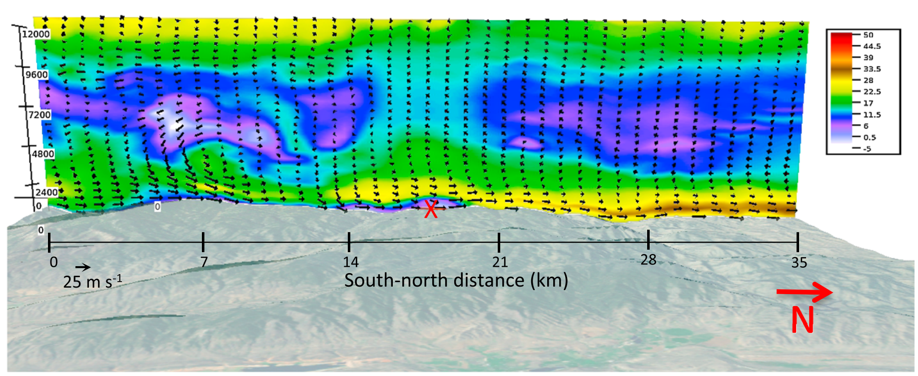

Figure 7. Vectors indicate simulated wind in a south-north vertical cross section through domain 4 through the ignition point, which is indicated in both figures with a red *X*. Wind speed perpendicular to the plane (from back to front, in m s^{-1}) at 17:20 UTC 9 June (11:20 A.M. MDT) (as in Figure 5b) contoured according to the color bar.

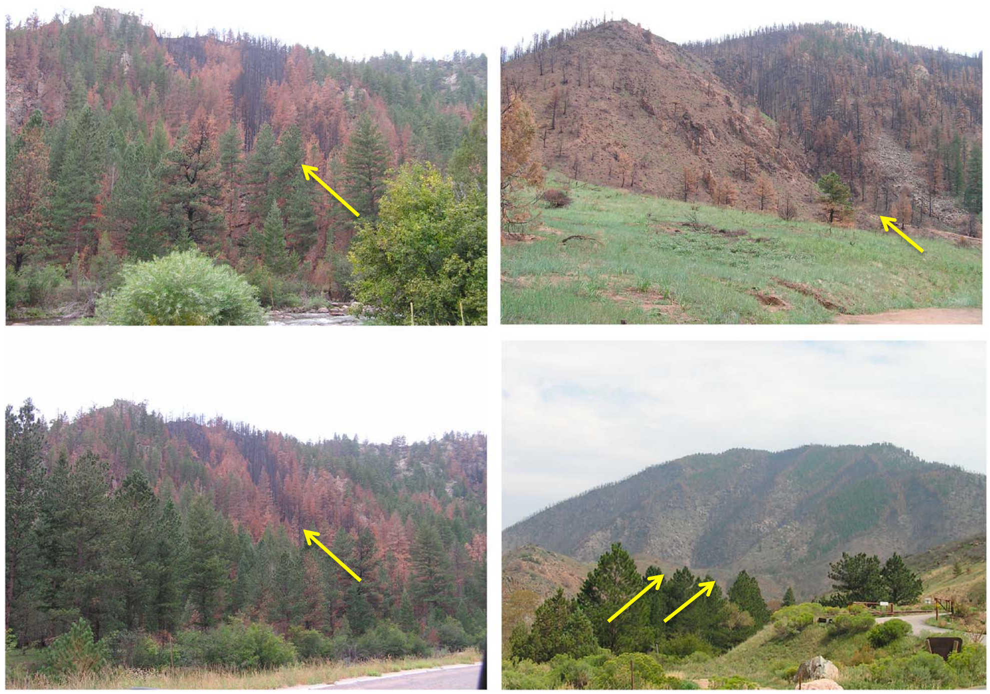

Figure 8. Photos showing high spatial variability in burn severity, concentrated in topographic drainages, or "chimneys" (indicated by yellow arrows) 2 months after the fire. In each figure, fire propagation was from the top of the ridge to bottom.

The leading edge of the simulated fire was accentuated by fine-scale fingers of locally high-fire heat flux a few hundred meters wide (e.g., Figures 6c and 6d), the finest scale that can be resolved with these simulations, which lead nearby points on the fire line. These fingers occurred where the fire growth aligned with a drainage, creating a "chimney effect" as the narrowing walls focus the inflow drawn into convection produced by the fire and locally increase winds over the fire line, accelerating it, and creating a larger burning area and thus an increased heat flux. This occurred particularly as the fire ascended drainages, but also as winds were channeled and accelerated between topographic features, even downslope. Photographs support the occurrence of intense burning where the fire is known to have burned down narrow chimneys, creating severely burned areas tens of meters wide between less burned and surviving trees (Figures 8a–8d). This rapid spread, causing a wide area to be burning at once, created locally enhanced heat fluxes and wind-aligned streaks in the simulated maximum total heat flux (i.e., including sensible and latent heat fluxes from both surface and crown fires) (Figure 9a). Based on visual comparison between satellite observations of fire intensity (the heat flux estimated from emissions in thermal bands) and burn severity [*Heward et al*., 2013], this model product may indicate some aspect of burn severity such as, in this case, the wide range of severity, visual similarity to the patchiness, and the size and orientation of elements of similar severity. For example, cigar-shaped streaks a few hundred meters wide, more intensely burned than their surroundings and aligned lengthwise parallel to the estimated direction of fire growth, particularly in topographic channels, appear both in model results (Figure 9a) and the incident's soil burn severity map (Figure 9b) (High Park Fire Burned Area Emergency Response (BAER) Report, Larimer County, CO, 35 pp., http://www.larimer.org/highparkfire/bear_report.pdf, 2012). However, visual comparison does not support one-to-one colocation of observed and modeled streaks. A more quantitative comparison cannot be done in this case because of limitations with the available satellite (Landsat 7) reference data. Fuel variations within the drainages have not been considered but could also contribute to this effect.

Additional experiments (listed in Table 1) indicated the sensitivity of simulated fire extent to horizontal grid resolution and fuel moisture. Experiment 4D_06_075 was similar to Experiment 5D_06_075 but refined only to four domains, with the same vertical grid but a deeper domain. Experiment 4D_06_075

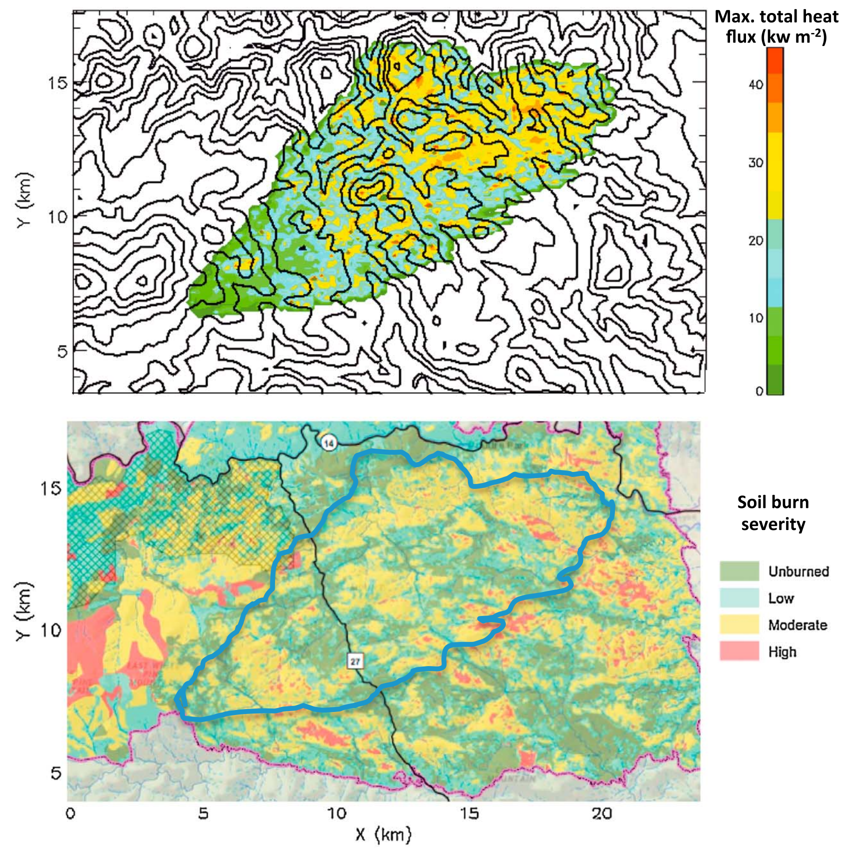

Figure 9. (a) The simulated maximum heat flux, including both surface and crown fire's sensible and latent heat fluxes. (b) The soil burn severity map from the High Park fire Burned Area Emergency Response (BAER) report (2012).

reproduced the same type of flow, including gravity waves over the Front Range and a sheltered area east of the ignition point, but the area sheltered from strong surface winds extended farther north. Despite the similarities, by 08:40 UTC 10 June (2:40 A.M. MDT), the simulated extent using 4D_06_074 was 9.4 km shorter than 5D_06_075 and lacked details such as turns in direction, splitting, or fingering at the leading edge (Figure 10). Nevertheless, because four versus five domains are about 18 times less computationally expensive, we used 4D_06_75 as a control experiment to test how variations in DFM and live fuel moisture (LFM) affected the results in four other experiments. Those fuel variations were applied uniformly across the domain as a proxy for the unknown spatial variability between measurements. Overall, changes in fuel moisture did not change the character of the outcomes but had modest impact on the extent of the fire's leading edge. For example, decreasing the dead fine fuel moisture from 6% to 4% in experiments with 75% LFM (4D_06_075 and 4D_04_075, respectively) increased the extent of the fire by 1 km or 11% and in the experiments with 90% LFM (4D_06_090 and 4D_04_090, respectively) by 2.4 km or 27%. Increasing the live fuel moisture from 75% to 90%, a value more representative of actual conditions, in the experiments with 4% DFM (4D_04_075 and 4D_04_090, respectively) increased fire extent by 1.4 km, a 14% increase, and made little change in the experiments (4D_06_075 and 4D_06_090, respectively) with 6% DFM. Counterintuitive results like the latter must be anticipated in dynamic models, as increased live fuel moisture will not only affect the algorithm controlling the transition from surface to crown fire but increase the latent heat flux to the atmosphere, plume buoyancy, and fire-induced winds. Assuming that it is captured in the change in fuel moisture conditions used in the simulations, the marginal impact of the drought on fire extent, determined by contrasting the prior experiments with 90% LFM to one with "moderately dry" conditions (4D_08_110), was to increase the simulated fire's extent between 0 and 3.4 km (0–39%). Drought conditions with additionally decreased live fuel moisture that might serve as a proxy for beetle kill increased simulated fire extent over the moderately dry configuration between 0.3 and 1.8 km (4–19%).

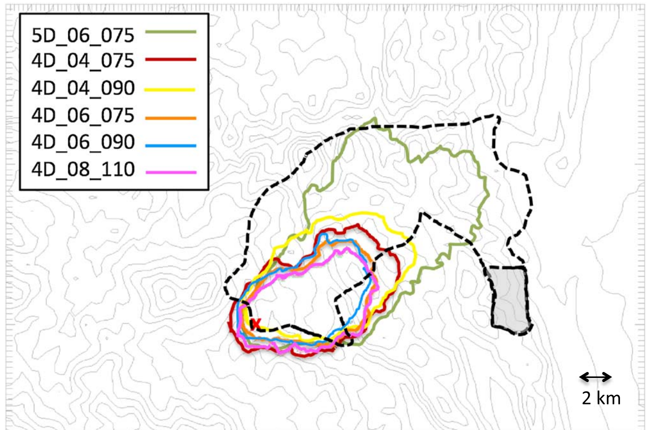

Figure 10. Simulated fire extent at 08:40 UTC 10 June (2:40 A.M. MDT) from six numerical experiments (solid lines, identified in Table 1) along with the incident team map of fire extent from approximately 4:00 to 5:00 A.M. 10 June. Terrain contours are plotted every 92 m. ***X*** indicates the ignition location.

5. Conclusions and Discussion

The 2012 High Park fire in Colorado had an extreme impact because of a combination of a climate and a wind-producing weather event, which led to rapid, damaging fire spread, in addition to its proximity to the wildland urban interface. This strongly resembled other recent wildfire events, although the windstorm was not typical of local climatology. This work aimed to analyze the first day's growth of the High Park fire, which occurred in Colorado's Front Range during widespread drought and an unseasonal June windstorm, test to what extent the CAWFE coupled numerical weather prediction—wildland fire behavior model can reproduce the event and burn severity patterns, and show how the event was impacted by the drought impact on fuel moisture.

CAWFE was used to simulate the weather in the fire environment, telescoping from the synoptic scale environment down to convective scale terrain-induced flow effects, the ignition and growth of the High Park fire in fuel conditions reflecting the widespread drought, and the weather-fire dynamic interactions during its first growth period. Simulation results showed that the airflow regime in this event was characterized by the formation and breaking of mountain gravity waves with three-dimensional, time-evolving features. As in *Clark et al*. [2000], capturing processes across spatial scales varying by a factor of approximately 100 (10,000 m to 123 m), from synoptic down to convective scale motions, was required to reproduce the variety of the windstorm dynamics, reproduce the general characteristics of the local flow, and in this work, model its impacts on fire growth. Details in vertical wind and thermal structure determined whether the environment could support vertical wave propagation and transport energy toward the surface, while high horizontal resolution was needed to capture the structure of overturning wave dynamics. As noted by *Peltier and Clark* [1979], such events are thought to be highly nonlinear, meaning that small perturbations can lead to dramatically different outcomes. Validating simulated flow in three-dimensional complex terrain with experimental data is extremely difficult even when the solution and error characteristics of sensors are known. The complexity of the flow and the limits to predictability of small-scale features suggested an approach aimed at reproducing the flow regime and the outcome on fire behavior and examining its sensitivity to model parameters pertinent to the study. However, the nonlinearity also precluded difference analyses between otherwise identical simulations with and without a fire that would reveal the feedback of the fire, because much of the large change that occurred cannot meaningfully be interpreted as a physical consequence of the fire.

During its initial development, the simulated fire grew slowly to the northeast, lying under the gravity wave crest or its descending region, sheltered from the windstorm's strong surface winds and driven by fluctuating weak gusts from upstream peaks to the southwest. Following this unanticipated early growth, its eastern flank ran east when exposed to the full strength of steady, strong downslope winds, driving it toward Fort Collins. These growth periods were supported by two 14–18 h long wind surges recorded by weather stations, in addition to satellite and airborne remote sensing active fire detection data, and incident management maps. Finer scales of motion had important impacts on the event, particularly the early growth period and features that developed along the evolving fire front when wind was funneled through narrow inclined drainages. The presence but not specific locations of fine-scale-simulated features are supported by maps of burn severity and the postfire forest photographs.

In seeking to anticipate and explain the event, operational tools and postfire reports emphasize the dominant large-scale flow and its expected broad, nonspecific impacts on the unfolding of the event, primarily because observational weather data in unplanned events are often sparse. For example, here, downwind stations could only confirm periods of strong, gusty surface winds in the foothills downwind of the fire and in cities farther east on the plains. Consequently, variation from those analyses and distinctive characteristics in the fire maps appear inexplicable and unpredictable. This and prior studies are showing some specific, detailed features that can be captured and possibly predicted, provided that crucial fire environment factors and their effects at multiple scales ranging from interannual precipitation anomalies to convective-scale motions of a few hundred meters are captured. In this study, these notably include changing of the orientation of synoptic winds with respect to the Rocky Mountains, atmospheric gravity wave steepening and breaking, and small flow effects that sheltered the fire in its early period, fingering along the leading edge, and streaks in the burn severity. Meanwhile, apparently important factors such as the marginal effect of the drought conditions on fire growth did not alter its character and showed inconclusive impact on the extent of fire growth. Small-scale variability in other fire environment factors such as the dead and live fuel moistures and variability in fuel properties within a single fuel model were not explicitly tested but could contribute to or detract from some noted effects such as streaks of simulated burn severity aligned within topographic drainages.

Doyle et al. [2000] compared 11 numerical models' two-dimensional simulations of gravity wave breaking during a Front Range windstorm and found that gravity wave breaking may be quite predictable in some situations. The models' ability to capture those events was impacted by numerical dissipation, numerical representation of horizontal advection, and lateral boundary conditions, and in contrast to the approximately 200 m used by those models, vertical resolution in operational models at the time was not enough. Simulating wave breaking in three dimensions over three-dimensional topography with evolving upwind boundary conditions is even more complex. This study further illuminates the characteristics that models require to simulate these combined windstorm-fire events. Our results echo previous coupled weather-fire model case studies that suggest that coupled weather-fire modeling requires modeling at horizontal grid spacing finer than the mesoscale, generally regarded as 1–10 km. A simulation employing 370 m horizontal grid spacing captured the overall direction and width of fire growth but missed potentially important features captured in the 123 m grid spacing simulation including a period during early growth of the fire to the north and fingering along the fire line. Applications of mesoscale models such as the Weather Research and Forecasting model to breaking gravity waves [*Rognvaldsson et al*., 2011; *Trier et al*., 2012] showed that such models only begin to capture some aspects of this flow as the grid spacing is decreased from 1 to 0.7 km horizontal grid spacing; fully resolving such flows requires resolution finer than the model's target horizontal grid resolutions of 1–10 km [*Klemp*, 2006]. In addition, the required horizontal grid spacing is finer than even the specialized NCEP North American Model 1.3 km operational fire weather grid developed to give guidance on weather near fires. Although mesoscale models have the necessary nonhydrostatic capabilities, the simulation scenario described in this study requires additional model characteristics to (i) capture flow in complex terrain with high slope and complexity without numerical instability, (ii) support vertical grid refinement to allow comparable vertical and horizontal grid dimensions when refining across spatial dimensions spanning a factor of 100, and (iii) use methods that minimize damping of fine-scale motions.

In addition, diagnostic wind tools such as Wind Wizard [*Butler et al*., 2006] are being used as input into fire growth tools. These are based on a subset of terms from the momentum equations, notably assuming thermal terms, temporal variability, and vertical transport of kinetic energy to the surface are negligible. In these conditions, however, all of which are key factors in the intrinsic time-varying nature, vertical motions, and thermal overrunning that characterize wave formation and breaking, as well as any fire-atmosphere feedback; thus, such tools cannot be expected to successfully represent airflow in these conditions. Similarly, probabilistic fire growth tools that rely on historical weather data such as FSPro (U.S. Department of Agriculture (USDA) Forest Service, Reference Guide: FSPro Overview 1.0, available from the U.S. Geological Survey at http://wfdss.usgs.gov/wfdss/pdfs/fspro_reference.pdf, 2009) would also have difficulty anticipating the actual outcome due to the unseasonal nature of the windstorm and local flow effects unique to each event.

Acknowledgments

The mesonet data are available from the University of Utah at http://mesowest.utah.edu. The fuel model data are available from the LANDFIRE program at http://www.landfire.gov. The NCEP final analyses are available for download from the National Oceanic and Atmospheric Administration at ftp://ftpprd.ncep.noaa.gov/pub/data/nccf/com/. The NARR imagery can be obtained at http://www.esrl.noaa.gov/psd/cgi-bin/data/narr/plothour.pl. The fuel moisture data are available from the Wildland Fire Assessment System at http://www.wfas.net. The terrain data were obtained from the U.S. Geological Survey, now available at http://nationalmap.gov. The VIIRS active fire data used in this study were generated by the authors using the algorithm described in *Schroeder et al*. [2014] and applied to input VIIRS sensor data record files downloaded from http://www.class.noaa.gov. Incident-specific information such as the fire extent data from NIROPS and the estimate from the incident management team, in addition to information on burning structures, were obtained from the multiagency incident management team and may be obtained from the authors. This work was supported by the National Aeronautics and Space Administration under awards NNX12AQ87G and NNH11AS03, the National Science Foundation (NSF) under grant 0835598, and the Federal Emergency Management Agency under award EMW-2011-FP-01124. The National Center for Atmospheric Research is sponsored by NSF. Any opinions, findings, and conclusions or recommendations expressed in this material are the authors' and do not reflect the views of NSF. We thank Chad Hoffman for providing the reports describing the High Park wildfire event, Kelly Close for discussions involving the event and the incident team fire map, Melvyn Shapiro for the helpful discussions regarding the event, and John Moody and Patricia Oliva for the discussions regarding burn severity. Comments from anonymous reviewers greatly improved the manuscript.

References

Albini, F. A. (1976), Estimating wildfire behavior and effects, in *USDA Forest Service Intermountain Forest and Range Experiment Station General, Tech. Rep. INT-30*, Ogden, Utah.

Anderson, H. E. (1982), Aids to determining fuel models for estimating fire behavior, in *Intermountain Forest and Range Experiment Station General, Tech. Rep. INT-122*, USDA Forest Service, Ogden, Utah.

Butler, B. W., M. Finney, L. Bradshaw, J. Forthofer, C. McHugh, R. Stratton, and D. Jimenez (2006), WindWizard: A new tool for fire management decision support, Conference Proceedings: Fuels Management—How to Measure Success, Portland, OR. Proceedings RMRS-P-41. U.S. Dep. of Agriculture, Forest Service, Rocky Mountain Research Station, 10 pp., 28–30 March.

Clark, T. L. (2003), Block-iterative method of solving the nonhydrostatic pressure in terrain-following coordinates: Two-level pressure and truncation error analysis, *J. Appl. Meteorol.*, *42*, 970–983.

Clark, T. L., and R. D. Farley (1984), Severe downslope windstorm calculations in two and three spatial dimensions using anelastic interactive grid nesting, *J. Atmos. Sci.*, *41*, 329–350.

Clark, T. L., and W. D. Hall (1991), Multi-domain simulations of the time-dependent Navier-Stokes equations: Benchmark error analysis of some nesting procedures, *J. Comput. Phys.*, *92*, 456–481.

Clark, T. L., and W. R. Peltier (1977), On the evolution and stability of finite-amplitude mountain waves, *J. Atmos. Sci.*, *34*, 1715–1730.

Clark, T. L., W. D. Hall, and R. M. Banta (1994), Two-and three-dimensional simulations of the 9 Jan 1989 severe Boulder windstorm: Comparison with observations, *J. Atmos. Sci.*, *51*, 2317–2343.

Clark, T. L., W. D. Hall, and J. L. Coen (1996), Source code documentation for the Clark-Hall Cloud-scale Model Code Version G3CH01, *Tech. Note NCAR/TN-426+STR*, doi:10.5065/D67W694V.

Clark, T. L., T. Keller, J. Coen, P. Neilley, H.-M. Hsu, and W. D. Hall (1997), Terrain-induced turbulence over Lantau Island: 7 June 1994 Tropical Storm Russ case study, *J. Atmos. Sci.*, *54*, 1795–1814.

Clark, T. L., W. D. Hall, R. M. Kerr, D. Middleton, L. Radke, F. M. Ralph, P. J. Neiman, and D. Levinson (2000), Origins of aircraft-damaging clear-air turbulence during the 9 December 1992 Colorado Downslope Windstorm: Numerical simulations and comparison with observations, *J. Atmos. Sci.*, *57*, 1105–1131, doi:10.1175/1520-0469(2000)057<1105:OOADCA>2.0.CO;2..

Clark, T. L., M. Griffiths, M. J. Reeder, and D. Latham (2003), Numerical simulations of grassland fires in the Northern Territory, Australia: A new subgrid-scale fire parameterization, *J. Geophys. Res.*, *108*(D18), 4589, doi:10.1029/2002JD003340.

Coen, J. L. (2005), Simulation of the Big Elk fire using coupled atmosphere-fire modeling, *Intl. J. Wildland Fire*, *14*, 49–59.

Coen, J. L. (2013), Modeling wildland fires: A description of the Coupled Atmosphere-Wildland Fire Environment model (CAWFE), *Tech. Note NCAR/TN-500+STR*, Natl. Cent. for Atmos. Res., Boulder, Colo., doi:10.5065/D6K64G2G.

Coen, J. L., and P. J. Riggan (2014), Simulation and thermal imaging of the 2006 Esperanza wildfire in southern California: Application of a coupled weather-wildland fire model, *Intl. J. Wildland Fire*, *23*, 755–770.

Coen, J. L., and W. Schroeder (2013), Use of spatially refined remote sensing fire detection data to initialize and evaluate coupled weather-wildfire growth model simulations, *Geophys. Res. Lett.*, *40*, 1–6, doi:10.1002/2013GL057868.

Coen, J. L., S. Mahalingam, and J. W. Daily (2004), Infrared imagery of crown-fire dynamics during FROSTFIRE, *J. Appl. Meteorol.*, *43*, 1241–1259.

Cotton, W. R., J. F. Weaver, and B. A. Beitler (1995), An unusual downslope wind event in Fort Collins, Colorado, on 3 July 1993, *Weather Forecasting*, *10*, 786–797.

Cruz, M. G., M. E. Alexander, and R. H. Wakimoto (2005), Development and testing of models for predicting crown fire rate of spread in conifer forest stands, *Can. J. For. Res.*, *35*, 1626–1639.

Doyle, J. D., et al. (2000), An intercomparison of model-predicted wave breaking for the 11 January 1972 Boulder windstorm, *Mon. Weather Rev.*, *128*, 901–914, doi:10.1175/1520-0493(2000)128<0901:AIOMPW>2.0.CO;2.

Heward, H., A. M. S. Smith, D. P. Roy, W. T. Tinkman, C. M. Hoffman, P. Morgan, and K. O. Lannom (2013), Is burn severity related to fire intensity? Observations from landscape scale remote sensing, *Intl. J. Wildland Fire*, *22*, 910–918, doi:10.1071/WF12087.

Hoffman, C. M., K. Pelz, J. Ziegler, and K. Moriarty (2012), Understanding the fire behavior and impacts of the High Park fire, paper presented at High Park Fire Symposium: From Science to Action and Recovery, Warner College of Natural Resources, Colorado State Univ., Fort Collins, Colo.

Jolly, W. M., R. A. Parsons, A. M. Hadlow, G. M. Cohn, S. S. McAllister, J. B. Popp, R. M. Hubbard, and J. F. Negron (2012), Relationships between moisture, chemistry, and ignition of *Pinus contorta* needles during the early stages of mountain pine beetle attack, *For. Ecol. Manage.*, *269*, 52–59.

Julian, L. T., and P. R. Julian (1969), Boulder's winds, *Weatherwise*, *22*, 109–112.

Klemp, J. B. (2006), Advances in the WRF model for convection-resolving forecasting, *Adv. Geosci.*, *7*, 25–29.

Lilly, D. K. (1978), A severe downslope windstorm and aircraft turbulence induced by a mountain wave, *J. Atmos. Sci.*, *35*, 59–77.

Lilly, D. K., and E. J. Zipser (1972), The Front Range windstorm of 11 January 1972: A meteorological narrative, *Weatherwise*, *25*, 56–63.

Mercer, A. E., M. B. Richman, H. B. Bluestein, and J. M. Brown (2008), Statistical modeling of downslope windstorms in Boulder, Colorado, *Weather Forecasting*, *23*, 1176–1194.

Parker, T. J., and T. P. Lane (2013), Trapped mountain waves during a light aircraft accident, *Aust. Meteorol. Oceanogr. J.*, *63*, 377–389.

Peltier, W. R., and T. L. Clark (1979), The evolution and stability of finite-amplitude mountain waves. Part II: Surface wave drag and severe downslope windstorms, *J. Atmos. Sci.*, *36*, 1498–1529.

Raphael, M. N. (2003), The Santa Ana winds of California, Earth Interactions, 7. [Available at http://EarthInteractions.org.]

Rognvaldsson, O., J.-W. Bao, H. Agustsson, and H. Olafsson (2011), Downslope windstorm in Iceland: WRF/MM5 model comparison, *Atmos. Chem. Phys.*, *11*, 103–120.

Rothermel, R. C. (1991), Predicting behavior and size of crown fires in the northern Rocky Mountains, Res. Paper INT-438. Ogden, UT: U.S. Dep. of Agriculture, Forest Service, Intermountain Forest and Range Experiment Station, 46 p.

Ryan, W., and N. Doesken (2012), Drought of 2012 in Colorado, Colorado Climate Center, Department of Atmospheric Science, Colorado State Univ., Fort Collins, Colo., 80523, 7 pp. [Available at http://ccc.atmos.colostate.edu/pdfs/climo_rpt_13_1.pdf.]

Schoennagel, T., T. T. Veblen, J. F. Negron, and J. M. Smith (2012), Effects of mountain pine beetle on fuels and expected fire behavior in lodgepole pine forests, Colorado, USA, *PLoS One*, *7*, e30002, doi:10.1371/journal.pone.0030002.

Schroeder, W., P. Oliva, L. Giglio, and I. Csiszar (2014), The new VIIRS 375 m active fire detection data product: Algorithm description and initial assessment, *Remote Sens. Environ.*, *143*, 85–96.

Scinocca, J. F., and W. R. Peltier (1989), Pulsating downslope windstorms, *J. Atmos. Sci.*, *46*, 2885–2914, doi:10.1175/1520-0469(1989)046<2885:PDW>2.0.CO;2.

Scott, J. H. (2006), Comparison of crown fire modeling systems used in three fire management applications, *Res. Pap. RMRS-RP-58*, 25 p., U.S. Dep. of Agric., For. Serv., Rocky Mountain Res. Stn., Fort Collins, Colo.

Sharman, R., W. D. Hall, T. Keller, and J. Wolff (2004), The operational prediction of mountain wave turbulence using a high resolution nonhydrostatic mesoscale model, paper presented at 11th Conference on Aviation, Range, and Aerospace Meteorology, Am. Meteorol. Soc. 4.12, Hyannis, Mass.

Taylor, S. W., B. M. Wotton, M. E. Alexander, and G. N. Dalrympole (2004), Variation in wind and crown fire behavior in a northern jack pine-black spruce forest, *Can. J. For. Res.*, *34*, 1561–1576.

Trier, S. B., R. D. Sharman, and T. P. Lane (2012), The influence of moist convection on a cold-season outbreak of near-cloud aviation turbulence, *Mon. Weather Rev.*, *140*, 2477–2496.

Van Wagner, C. E. (1977), Conditions for the start and spread of crown fire, *Can. J. For. Res.*, *7*, 23–34.

Whiteman, C. D., and J. G. Whiteman (1974), An historical climatology of damaging downslope windstorms at Boulder, Colorado, *NOAA Tech. Rep. ERL 336-APCL,* 68 pp., Natl. Oceanic Atmos. Admin., Boulder, Colo.

